

Article

Advanced Hysteretic Model of a Prototype Seismic Isolation System Made of Polymeric Bearings

Tomasz Falborski *  and Robert Jankowski 

Faculty of Civil and Environmental Engineering, Gdansk University of Technology, 11/12 Narutowicza St., 80-233 Gdansk, Poland; jankowr@pg.gda.pl

* Correspondence: tomfalbo@pg.gda.pl; Tel.: +48-58-347-21-17

Received: 12 January 2018; Accepted: 6 March 2018; Published: 9 March 2018

Featured Application: An advanced mathematical model to simulate complex hysteretic behaviour of a prototype seismic isolation system made of Polymeric Bearings in numerical simulations of base-isolated structures.

Abstract: The present paper reports the results of a comprehensive study designed to verify the effectiveness of an advanced mathematical model in simulating the complex mechanical behaviour of a prototype seismic isolation system made of polymeric bearings (PBs). Firstly, in order to construct the seismic bearings considered in this research, a specially prepared flexible polymeric material with increased damping properties was employed. High effectiveness of PBs in reducing structural vibrations due to seismic excitations was already confirmed during a previously conducted shaking table investigation. In order to accurately capture the complex mechanical behaviour of PBs in numerical analysis, the proposed mathematical model defines the lateral force as a nonlinear function of shear displacement and deformation velocity. Function parameters were evaluated by fitting the general form of the mathematical model into the experimentally obtained hysteresis loops, using the least squares optimisation method. The effectiveness of the mathematical model was verified by comparing the experimental data (i.e., seismic response of a 1.20 m high single-storey and a 2.30 m high two-storey structure models under various ground motions) with the results obtained from the detailed numerical analysis, where the experimental models were idealized as multi-degree-of-freedom systems. The results obtained from this investigation explicitly confirmed that the proposed mathematical model can be successfully adopted to accurately capture complex mechanical behaviour of PBs in numerical studies.

Keywords: hysteretic behaviour; polymeric bearings; base isolation; seismic performance; dynamic excitations

1. Introduction and Motivation

Earthquake-induced ground motions are identified as one of the most unpredictable, and more importantly, destructive threats to civil engineering structures. Strong seismic events may cause loss of life and property damage through soft-storey and weak-storey failures, pounding-induced damage (see, for example, [1,2]), brittle fracture and collapse of masonry and concrete structures, or failures resulting from excessive plastic deformations in steel frame structures. Therefore, developing earthquake protection systems in order to improve safety and reliability of structures is an issue of the highest priority in many seismically active regions (see, for example, [3,4]).

In general, the family of earthquake protective systems consists of passive, active, and semi-active (hybrid) control systems. Base isolation, which is an example of passive control methods, is recognized as one of the most effective and widely adopted approaches of protecting structures during strong ground motions (see, for example, [5,6]). This solution is also considered to be the safest and most reliable method,

because, in contrast to active and hybrid (semi-active) devices (see, for example, [7–9]), its activation requires no external source of energy, that may not necessarily be accessible due to earthquake-induced devastation. Broadly, base isolation system works by decoupling the building from the horizontal components of an earthquake ground motion by incorporating a layer with relatively low horizontal stiffness between the structure and its foundation (see, for example, [10–12]). Thus, the primary concept of base isolation systems is to modify structural dynamic properties by elongating the fundamental period of vibration and introducing additional damping so that base-isolated structures may respond more favourably to earthquake ground motions (see, for example, [13,14]). The philosophy of base isolation is well established and commonly accepted in many seismically active regions including California, Japan, and New Zealand. Base isolators, such as lead-rubber bearings (LRBs), high-damping rubber bearings (HDRBs), and friction pendulum bearings (FPBs), are commonly used in practice in order to improve structural safety, and thus, minimize property damage. It should also be mentioned, however, that base isolation devices made with the use of rubbery materials may be susceptible to aging resulting in degradation of stiffness and damping properties. Therefore, every type of rubber bearing requires routine maintenance to ensure the structural safety and reliability.

Both numerical and experimental results of research focused on the effectiveness of various types of base isolation system have been widely published (see, for example, [15–18]). More importantly, many of the completed base-isolated buildings have already experienced strong ground motions, and their dynamic performance has been just as predicted, which explicitly confirms high effectiveness of base isolation systems in suppressing structural vibrations (see, for example, [19,20]).

However, in order to get an accurate insight into the seismic performance of base-isolated structures in numerical analysis, it is absolutely necessary to accurately capture the mechanical behaviour of base isolation system. This issue is particularly important at the design stage of new structures or retrofitting existing ones. Moreover, with the increasing number of base isolators exhibiting different mechanical behaviour, which may also be triggered due to new materials employed, this task is very challenging and often requires an individual approach to a specific type of seismic isolation device. In nonlinear structural dynamics, there are generally a few approaches, which can be incorporated to simulate the nonlinear behaviour of base isolation devices. These mathematical models, however, are evaluated for different base isolators, which are characterized by their own specific load-displacement behaviour, and thus, may not be fully appropriate for detailed numerical analysis of structures isolated with different types of base isolation systems. Moreover, most of these models refer to either elastomeric bearings (see, for example, [21–24]), or HDRBs (see, for example, [25,26]), which are also susceptible to vertical loads.

Motivated by the preceding discussion, the present paper was designed to verify the effectiveness of an advanced hysteretic model in simulating complex force-deformation behaviour of a prototype seismic isolation system made of PBs, which are constructed with the use of a specially prepared for this purpose polymeric material with improved damping properties [27]. High effectiveness of PBs in reducing structural vibrations due to seismic excitations was confirmed during previously conducted extensive shaking table investigation and the results have already been published (see [28] for details). In order to achieve the above-mentioned aim of the present investigation, the following specific objectives were established:

- (1) Perform dynamic oscillatory test in order to determine the energy dissipation properties of the base isolation system made of PBs based on the experimentally obtained hysteresis loops.
- (2) Propose a general form of an advanced mathematical model, which defines the lateral force as a nonlinear function of shear displacement and deformation velocity, in order to accurately capture the nonlinear mechanical behaviour of PBs in numerical analysis of base-isolated structures.
- (3) Evaluate the function parameters by fitting the general form of the proposed mathematical model into the experimentally obtained hysteresis loops using the least squares optimisation method.
- (4) Implement the proposed mathematical model into the computational analysis in order to perform numerical evaluation of the seismic response of the previously examined experimental models

with dynamic characteristics typical for low-rise and medium-rise buildings, both fixed-base and base-isolated with the use of PBs, to a number of different ground motions and a mining tremor.

- (5) Verify the effectiveness of the proposed mathematical model in simulating nonlinear behaviour of PBs by comparing the results of the detailed lumped-parameter analysis with the experimentally obtained shaking table data.

2. Polymeric Bearings and Previous Shaking Table Investigation

Precise description of PBs, detailed material testing (i.e., static tension and compression tests, Dynamic Mechanical Analysis, etc.), and finally the results of the extensive shaking table investigation, which was conducted in order to verify the effectiveness of this prototype base isolation system in reducing structural vibrations due to ground motions, has already been published (see [27,28]). To briefly outline the key results it should be mentioned that PBs were constructed with the use of a specially prepared for this purpose polymeric material with increased energy dissipation potential. Energy dissipation potential of PBs was confirmed by a relatively high value of the loss factor obtained from the Dynamic Mechanical Analysis test. Moreover, static tension and compression results explicitly demonstrated that the tested polymer is considerably nonlinear and its mechanical behaviour is strongly dependent on the strain rate.

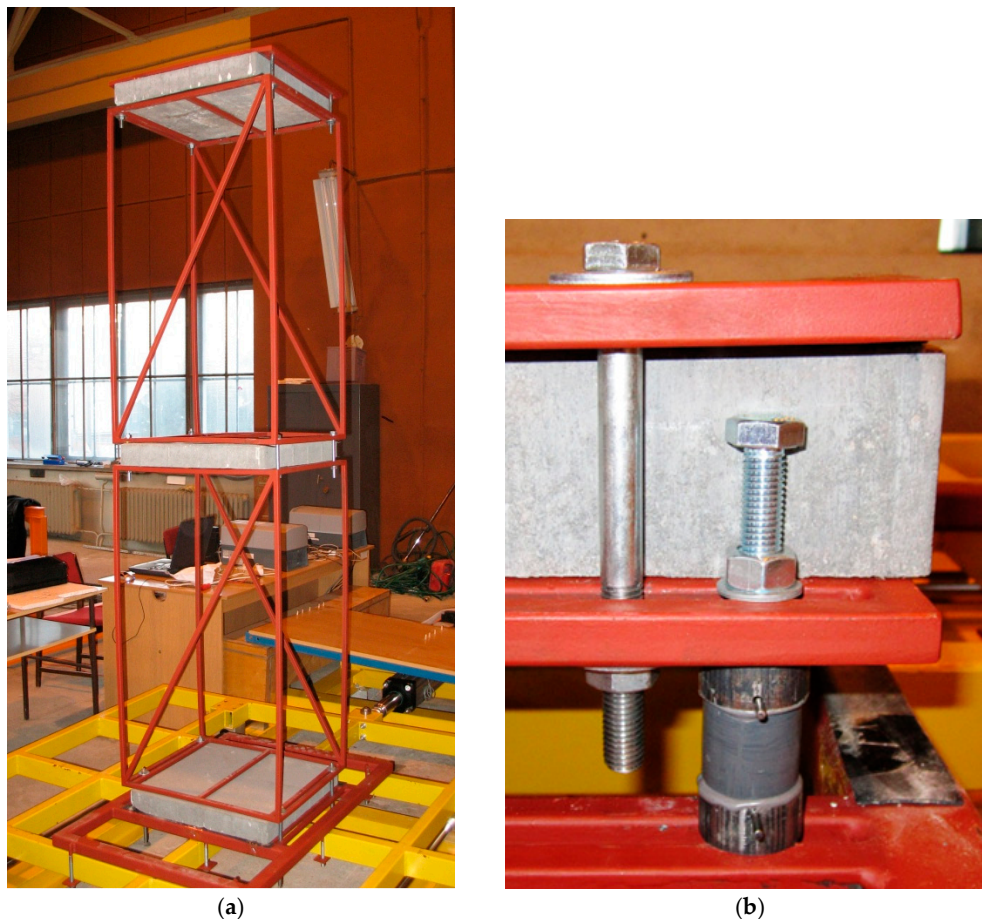


Figure 1. Shaking table investigation: fixed-base two storey experimental model (a) close-up view of PB used in base-isolated model (b).

In the final step, an extensive shaking table investigation was conducted. This experimental research program was performed with the use of a middle-sized one-directional shaking table platform, which was employed to simulate the lateral forces and displacements caused by seismic excitations.

Dynamic response of two experimental structure models with dynamic characteristics typical for low-rise and medium-rise buildings (i.e., a 1.20 m high single-storey, and a 2.30 m high two-storey structures with fundamental frequencies of 3.34 Hz and 1.94 Hz, respectively), both fixed-base and base-isolated with the use of PBs, to a number of different ground motions and a mining tremor (as an example of so-called induced seismicity) was deeply analyzed. As an example, the 2.30 m high two-storey experimental model mounted on the shaking table platform, together with the close-up view of PB, is presented in Figure 1. The results of this experimental research explicitly confirmed the effectiveness of seismic isolation system made of PBs in mitigating seismic-induced structural vibrations. Peak lateral accelerations recorded at the top of the tested structures subjected to a number of different ground motions were decreased by approximately 11–39% and 12–57% for the single-storey and two-storey structure models, respectively. Also, it is worth mentioning that a full scale version of the PB to be used for real structures was developed, submitted to the Polish Patent Office and patented in 2017.

3. Dynamic Oscillatory Test

The first step in the present research was to perform dynamic oscillatory tests in order to analyze the load-deformation behaviour of PBs under different horizontal excitation frequencies. In order to obtain hysteresis loops, four PBs supporting a concrete slab (dimensions of the concrete base slab are 50 cm × 50 cm × 7 cm), were mounted on the shaking table platform and subjected to harmonic excitations with gradually increasing amplitudes resulting in different shear strain levels. The experimental testing was carried out at the excitation frequencies of 1 Hz, 2 Hz, and 5 Hz, which correspond to the range of excitation frequencies typical for earthquakes and mining tremors. The response of the system to cyclic horizontal loading was measured using a laser displacement sensor and an uniaxial accelerometer, as indicated by Figure 2.

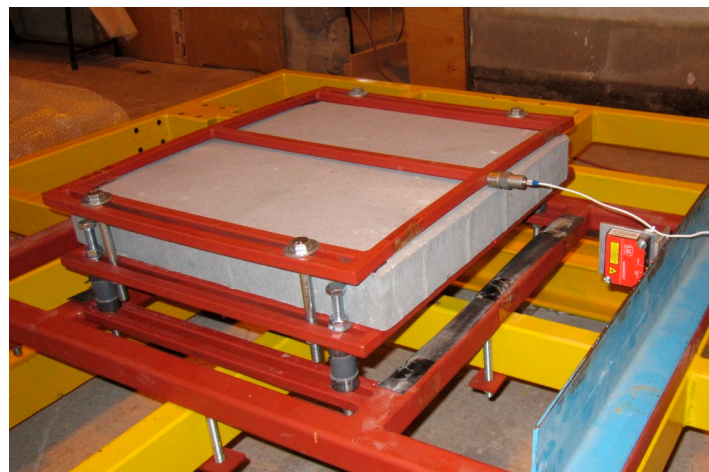


Figure 2. Base-isolated concrete slab during dynamic oscillatory test.

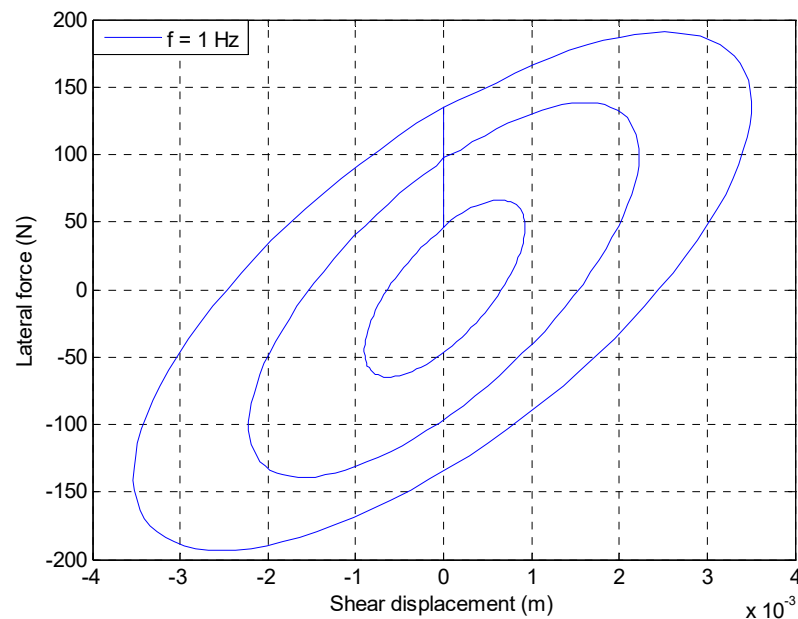
Experimentally obtained hysteresis loops for three different excitation frequencies are presented in Figure 3 (it should be mentioned that due to technical restrictions of the shaking table, limited number of hysteresis loops at the excitation frequency of 1 Hz could be obtained). Based on the loops, the equivalent damping ratio, ξ , of the base isolation system was determined using the following formula (see [26]):

$$\xi = \frac{\Delta W}{2\pi \cdot W} \quad (1)$$

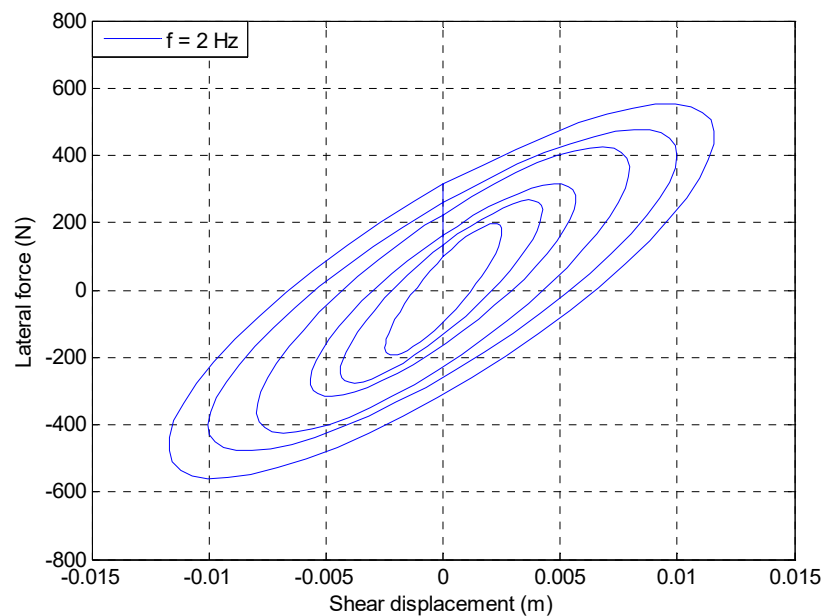
where ΔW is the energy dissipated in one cycle of motion (the area enclosed by the hysteresis loop) and W is a strain energy induced in a seismic isolation bearing given by:

$$W = F(u) \cdot u \quad (2)$$

where u is a maximum shear deflection and $F(u)$ is a lateral force recorded at u . Average values of equivalent damping ratios for hysteresis loops, recorded at three excitation frequencies, are briefly summarized in Table 1.



(a)



(b)

Figure 3. Cont.

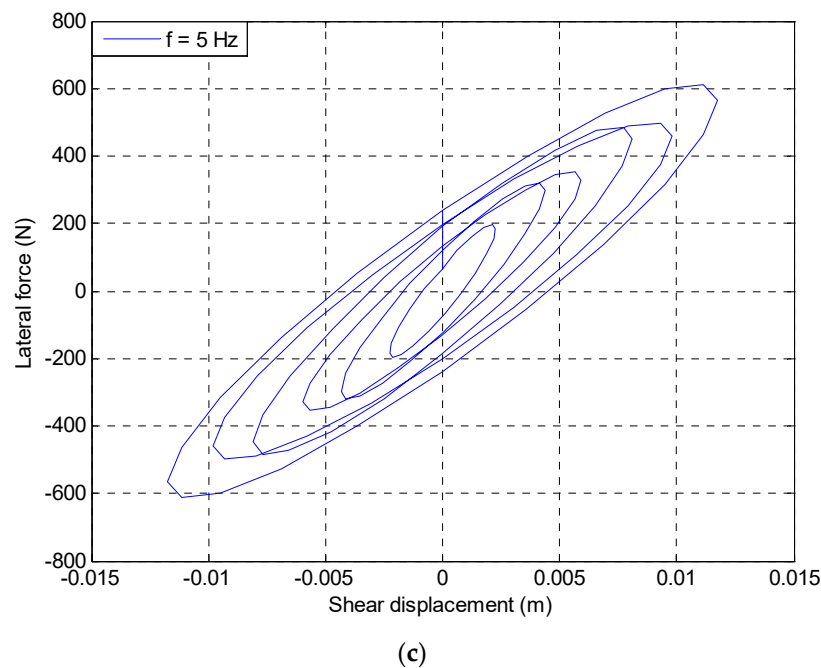


Figure 3. Experimentally obtained hysteresis loops at excitation frequencies of 1 Hz (a); 2 Hz (b); and 5 Hz (c).

Table 1. Average equivalent damping ratios.

Excitation Frequency	Damping Ratio, ξ
1 Hz	49.5%
2 Hz	30.5%
5 Hz	20.4%

The results obtained from the dynamic oscillatory tests exhibit pronounced hysteretic behaviour of PBs, which confirms high energy dissipation properties of this base isolation system. Moreover, experimentally obtained hysteresis loops indicate that PBs exhibit higher stiffness at lower shear strain levels. Close inspection of Figure 3 shows that with increasing shear deflection, the slope of the hysteresis loop decreases. The same effect, which is often referred to as the stiffness degradation, can also be observed for other seismic isolation devices, such as HDRBs [12]. Additionally, results obtained from this investigation clearly demonstrate that the higher the excitation frequency, the lower the value of equivalent damping ratio, ξ , as indicated by Table 1. The cyclic loading tests indicate that the damping ratio provided by PBs is within the range of about 20–49%, while for the most commonly used base isolators (LRBs, HDRBs, FPBs), the damping ratio is approximately 10–20%.

4. Mathematical Model

In order to accurately simulate the complex mechanical behaviour of PBs under lateral dynamic excitations in numerical analysis, an advanced hysteretic model was firstly developed. The general form of this mathematical model is presented in Equations (3)–(5). It defines the lateral force, F_b , as a nonlinear function of the shear displacement, $u_b(t)$, and the deformation velocity, $\dot{u}_b(t)$. In the proposed mathematical approach k_b , and c_b represent the stiffness and damping of the PBs, respectively. Function parameter a_1 defines the initial stiffness of PBs, parameter a_2 depicts stiffness degradation for higher strain rates (i.e., deformation velocity), parameters a_3 and a_4 are responsible for broadening and rounding hysteresis loops. Finally, parameter a_5 defines damping properties of PBs. The function

parameters a_1 – a_5 can be estimated by curve fitting the general form of the mathematical model to the experimentally obtained hysteresis loops using the least squares optimization method.

$$F_b(u_b(t), \dot{u}_b(t)) = k_b(u_b(t), \dot{u}_b(t)) \cdot u_b(t) + c_b \cdot \dot{u}_b(t) \quad (3)$$

$$k_b(u_b(t), \dot{u}_b(t)) = a_1 + \frac{a_2}{\cosh[a_3 \dot{u}_b(t)] \cdot \cosh[a_4 u_b(t)]} \quad (4)$$

$$c_b = a_5 \quad (5)$$

In the present study, the curve fitting procedure was conducted for hysteresis loops with different excitation frequencies and the exemplary results for the frequency of 2 Hz are shown below. The evaluated set of function parameters is summarized in Table 2. Comparison between experimentally and numerically obtained hysteresis loops is presented in Figure 4. It should be underlined that the normalized mean square error calculated for the fit is equal to 4.44%.

Table 2. Estimated values for function parameters for loops at excitation frequency of 2 Hz.

Function Parameter	Estimated Value	Unit
a_1	38.657	$\text{N} \cdot \text{m}^{-1}$
a_2	36.301	$\text{N} \cdot \text{m}^{-1}$
a_3	23.253	$\text{s} \cdot \text{m}^{-1}$
a_4	331.626	m^{-1}
a_5	2.1932	$\text{kg} \cdot \text{s}^{-1}$

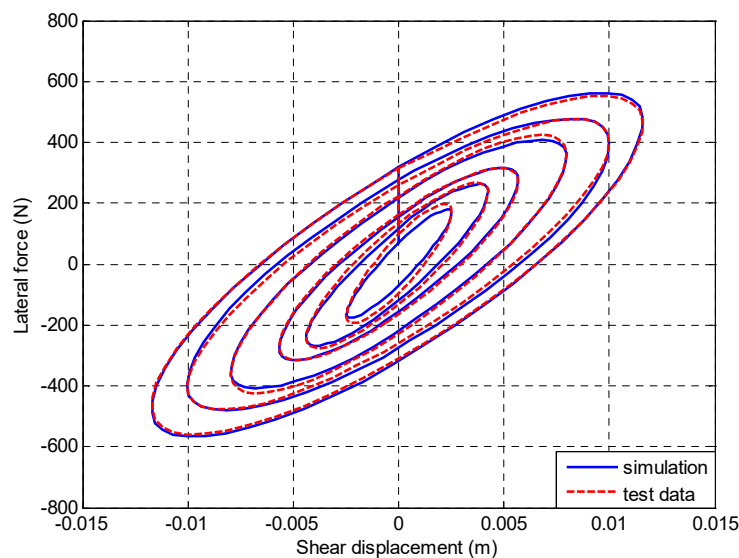


Figure 4. Experimental and numerical hysteresis loops at excitation frequency of 2 Hz.

5. Numerical Analysis

The final stage of the current investigation was focused on implementing the proposed mathematical model of PBs into detailed lumped-parameter numerical analysis (see, for example, [29]). Therefore, in order to verify the effectiveness of the proposed hysteretic model, the dynamic response of a single-storey and two-storey structure models, both fixed-base and base-isolated with PBs, to a number of ground motions was evaluated and compared to the previously obtained experimental data. The fixed-base and base-isolated single-storey structure models were idealized as a single-degree-of-freedom (1-DOF), and two-degree-of-freedom (2-DOF) systems, respectively. Consequently, the fixed-base and base-isolated two-storey structures were modelled

as a two-degree-of-freedom (2-DOF), and three-degree-of-freedom (3-DOF) systems, respectively. Two numerical models, each with and without base-isolation system, were subjected to the El Centro earthquake of 1940, the San Fernando earthquake of 1971, the Loma Prieta earthquake of 1989, the Northridge earthquake of 1994, and finally the Polkowice (Poland) tremor of 2002 as an example of mining-induced seismicity, which is also a major concern of professional and research communities (see, for example, [30,31]). For numerical evaluation of differential equation of motion, the unconditionally stable Newmark's average acceleration method was applied [29], as it is the most frequently adopted integration procedure in seismic analysis of structures.

5.1. Single-Storey Structure Model

In order to evaluate dynamic response of the fixed-based single-storey model in numerical analysis, the structure was idealized as 1-DOF system, for which the differential equation of motion is given in Equation (6). This simple numerical model is characterized by three parameters: lumped mass m_1 lumped at the roof level (i.e., first storey level), lateral stiffness k_1 , and viscous damping c_1 . The exact values of these parameters, which are also given in Equations (7)–(9), were already determined during the previously conducted shaking table investigation (see [28] for details):

$$m_1 \cdot \ddot{u}(t) + c \cdot \dot{u}(t) + k_1 \cdot u(t) = -m_1 \cdot \ddot{u}_g(t) \quad (6)$$

$$\omega = 2 \cdot \pi \cdot f \quad (7)$$

$$k_1 = \omega^2 \cdot m_1 \quad (8)$$

$$c_1 = 2 \cdot m_1 \cdot \omega \cdot \xi \quad (9)$$

Employing parameters determined in the previous study ([28]), i.e., dominant frequency of the fixed-base single-storey structure, f , equal to 3.34 Hz (and, consequently, angular frequency, ω , equal to 20.98 rad^{-1} according to Equation (7)), lumped-mass concentrated at the top level, m_1 , equal to 46.76 kg, and damping ratio, ξ , equal to 0.5%, into the Equations (8) and (9), stiffness and damping was obtained as $k_1 = 20,571 \frac{\text{N}}{\text{m}}$ and $c_1 = 10.48 \frac{\text{kg}}{\text{s}}$, respectively.

The single-storey structure model mounted on the foundation base plate supported with PBs (as shown in Figure 2) was considered as 2-DOF system, for which the differential equation of motion can be presented in a general matrix form given in Equation (10).

$$\mathbf{M} \cdot \ddot{\mathbf{u}}(t) + \mathbf{C} \cdot \dot{\mathbf{u}}(t) + \mathbf{K} \cdot \mathbf{u}(t) = -\mathbf{M}\mathbf{I} \cdot \ddot{u}_g(t) \quad (10)$$

In this formula, \mathbf{M} , \mathbf{C} , and \mathbf{K} denote mass, damping, and stiffness matrices, respectively, $\ddot{\mathbf{u}}(t)$, $\dot{\mathbf{u}}(t)$, $\mathbf{u}(t)$ are the acceleration, velocity and displacement vectors, respectively, and $\ddot{u}_g(t)$ stands for the acceleration input ground motion. Additional matrix \mathbf{I} is the influence coefficient matrix, having 1 for elements corresponding to degrees of freedom in the direction of the applied ground motion and 0 for other degrees of freedom. The structure was mounted on a base plate of mass m_b which is supported on a base isolation system made of PBs characterized by lateral stiffness $k_b(u_b(t), \dot{u}_b(t))$, and viscous damping c_b , as defined in Equations (4) and (5). Accordingly, for the base-isolated single-storey model idealized as 2-DOF system, matrices \mathbf{M} , \mathbf{C} , \mathbf{K} , $\ddot{\mathbf{u}}(t)$, $\dot{\mathbf{u}}(t)$, $\mathbf{u}(t)$ and \mathbf{I} are defined in Equations (11)–(15).

$$\mathbf{M} = \begin{bmatrix} m_b & 0 \\ 0 & m_1 \end{bmatrix} \quad (11)$$

$$\mathbf{C} = \begin{bmatrix} c_b + c_1 & -c_1 \\ -c_1 & c_1 \end{bmatrix} \quad (12)$$

$$\mathbf{K} = \begin{bmatrix} k_b(u_b(t), \dot{u}_b(t)) + k_1 & -k_1 \\ -k_1 & k_1 \end{bmatrix} \quad (13)$$

$$\mathbf{I} = \begin{Bmatrix} 1 \\ 1 \end{Bmatrix} \quad (14)$$

$$\ddot{\mathbf{u}}(t) = \begin{Bmatrix} \ddot{u}_b(t) \\ \ddot{u}_1(t) \end{Bmatrix}, \dot{\mathbf{u}}(t) = \begin{Bmatrix} \dot{u}_b(t) \\ \dot{u}_1(t) \end{Bmatrix}, \mathbf{u}(t) = \begin{Bmatrix} u_b(t) \\ u_1(t) \end{Bmatrix} \quad (15)$$

Numerically obtained acceleration-time history plots for the single-storey structure model, both fixed-base and base-isolated considered as 1-DOF and 2-DOF systems, respectively, are compared with the experimental data (see [28]) in Figures 5 and 6. Moreover, computed peak lateral accelerations recorded at the top of the analyzed single-storey structure model, with and without the PBs, are briefly reported in Table 3. Additionally, reduction levels in lateral accelerations are also presented and compared with the results of the previously performed shaking table investigation [28].

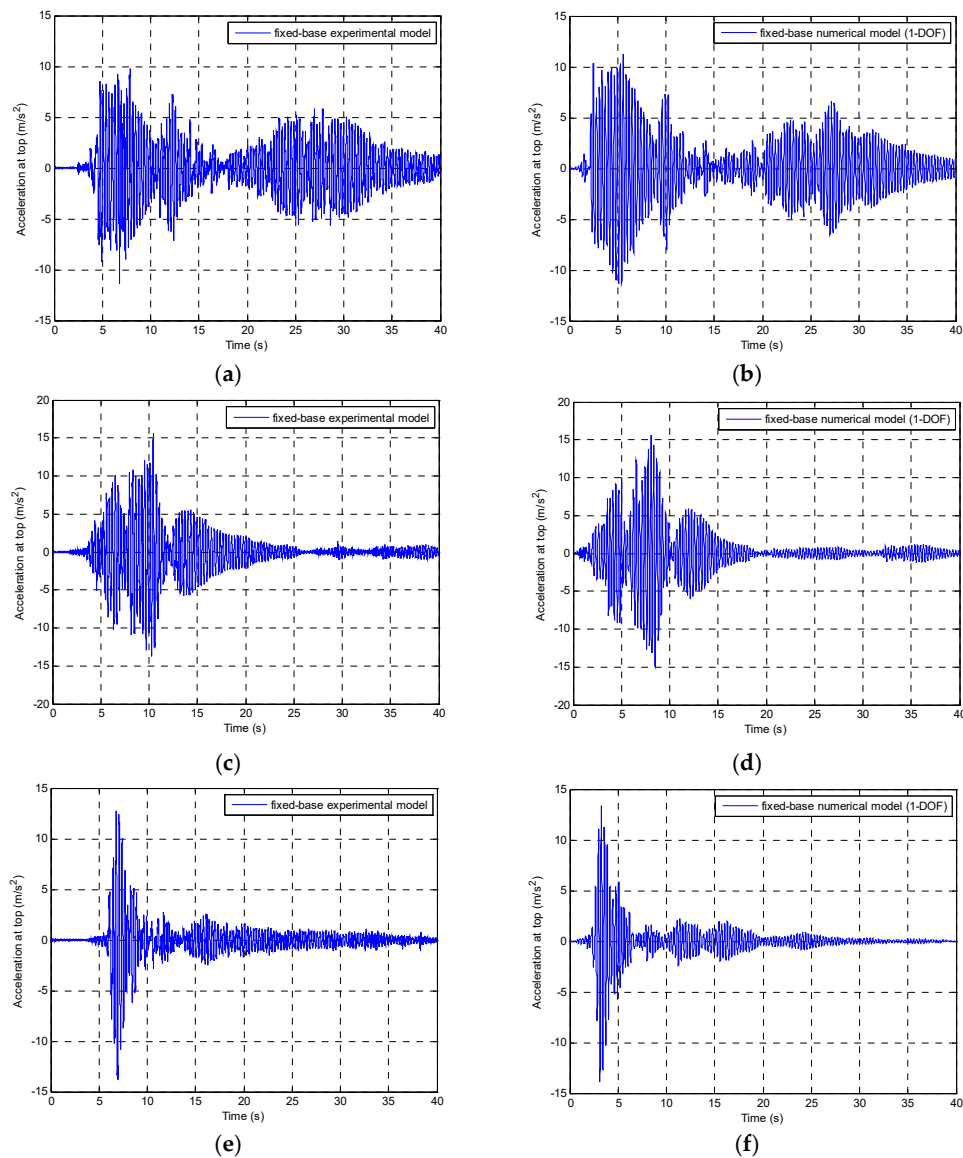


Figure 5. Cont.

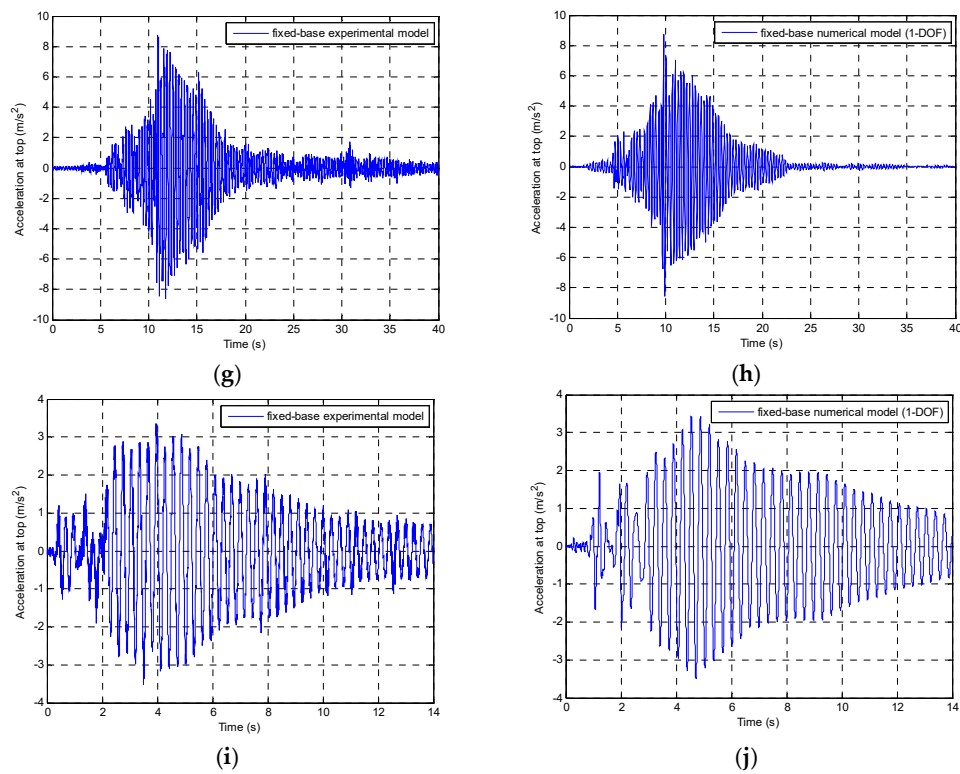


Figure 5. Experimentally determined (left) and numerically obtained (right) time-acceleration history plots for the fixed-base single-storey model during different ground motions: the 1940 El Centro earthquake (a,b), the 1971 San Fernando earthquake (c,d), the 1989 Loma Prieta earthquake (e,f), the 1994 Northridge earthquake (g,h), and the 2002 Polkowice mining tremor (i,j).

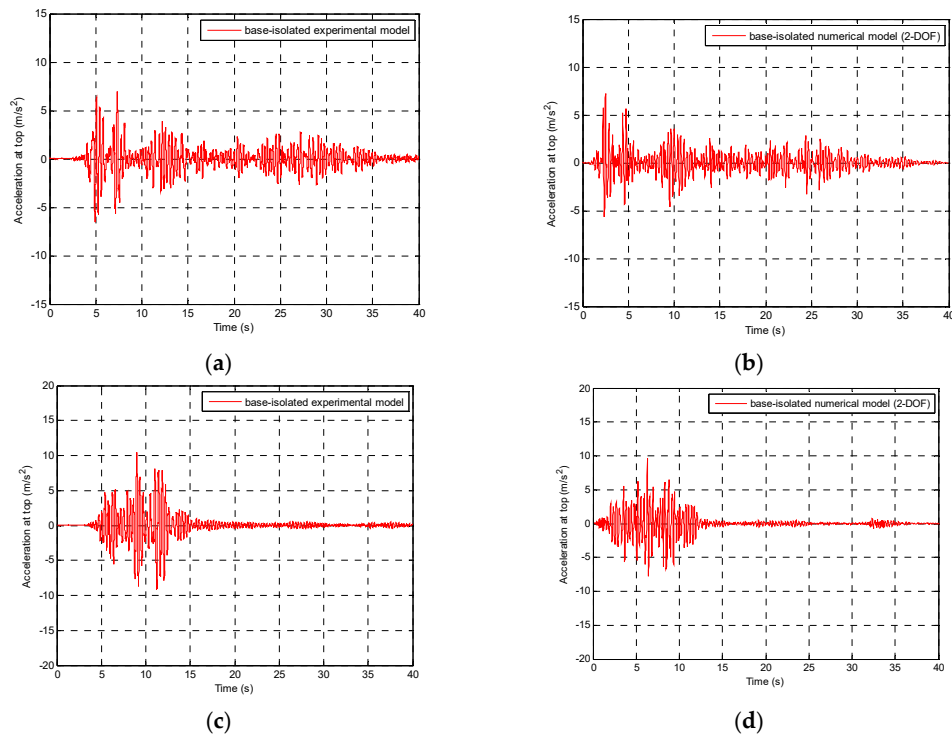


Figure 6. Cont.

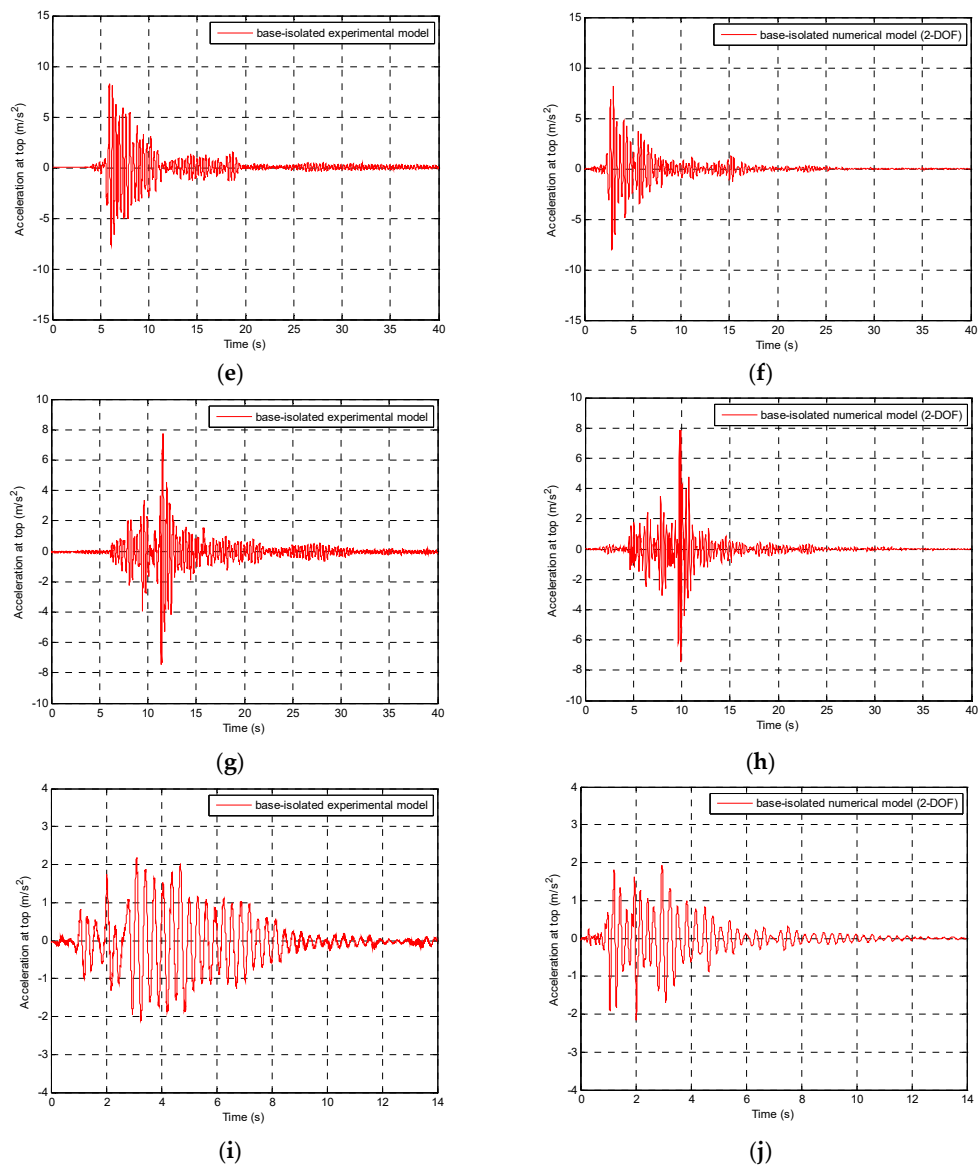


Figure 6. Experimentally determined (**left**) and numerically obtained (**right**) time-acceleration history plots for the base-isolated single-storey model during different ground motions: the 1940 El Centro earthquake (**a,b**), the 1971 San Fernando earthquake (**c,d**), the 1989 Loma Prieta earthquake (**e,f**), the 1994 Northridge earthquake (**g,h**), and the 2002 Polkowice mining tremor (**i,j**).

Table 3. Results of the seismic tests for the single-storey structure model.

Dynamic Excitation	Numerically Computed Peak Lateral Acceleration for the Single-Storey Structure Model (m/s^2)		Reduction Based on Numerical Analysis (%)	Reduction Based on Shaking Table Investigation (%) [28]
	Fixed-Base (1-DOF System)	Base-Isolated (2-DOF System)		
1940 El Centro earthquake NS component, original record with $\text{PGA} = 3.070 \text{ m/s}^2$	11.39	7.21	36.70	38.7
1971 San Fernando earthquake Pacoima Dam station, $\text{N}74^\circ\text{E}$ component, scaled record with $\text{PGA} = 5.688 \text{ m/s}^2$	15.64	9.66	38.24	32.8

Table 3. Cont.

Dynamic Excitation	Numerically Computed Peak Lateral Acceleration for the Single-Storey Structure Model (m/s ²)		Reduction Based on Numerical Analysis (%)	Reduction Based on Shaking Table Investigation (%) [28]
	Fixed-Base (1-DOF System)	Base-Isolated (2-DOF System)		
1989 Loma Prieta earthquake Corralitos station, NS component, scaled record with PGA = 3.158 m/s ²	13.86	8.16	41.16	40.2
1994 Northridge earthquake Santa Monica station, EW component, scaled record with PGA = 4.332 m/s ²	8.73	7.85	10.08	11.3
2002 Polkowice mining tremor NS component, original record with PGA = 1.634 m/s ²	3.50	2.17	38.00	38.2

Where: PGA: Peak Ground Acceleration, NS: North-South, EW: East-West.

5.2. Two-Storey Structure Model

In the next step of the numerical investigation, 2-DOF and 3-DOF systems were applied to simulate the dynamic behaviour of the fixed-base and base-isolated two-storey structure models, respectively. The general matrix form of differential equation of motion has already been presented in Equation (10). Similarly to the single-storey structure model, for the fixed-based two-storey structure model, matrices \mathbf{M} , \mathbf{C} , \mathbf{K} , $\ddot{\mathbf{u}}(t)$, $\dot{\mathbf{u}}(t)$, $\mathbf{u}(t)$ and \mathbf{I} are defined as given in Equations (16)–(20), whereas for the base-isolated case, these matrices are presented in Equations (21)–(25):

$$\mathbf{M} = \begin{bmatrix} m_1 & 0 \\ 0 & m_2 \end{bmatrix} \quad (16)$$

$$\mathbf{C} = \begin{bmatrix} c_1 + c_2 & -c_2 \\ -c_2 & c_2 \end{bmatrix} \quad (17)$$

$$\mathbf{K} = \begin{bmatrix} k_1 + k_2 & -k_2 \\ -k_2 & k_2 \end{bmatrix} \quad (18)$$

$$\mathbf{I} = \begin{Bmatrix} 1 \\ 1 \end{Bmatrix} \quad (19)$$

$$\ddot{\mathbf{u}}(t) = \begin{Bmatrix} \ddot{u}_1(t) \\ \ddot{u}_2(t) \end{Bmatrix}, \dot{\mathbf{u}}(t) = \begin{Bmatrix} \dot{u}_1(t) \\ \dot{u}_2(t) \end{Bmatrix}, \mathbf{u}(t) = \begin{Bmatrix} u_1(t) \\ u_2(t) \end{Bmatrix} \quad (20)$$

$$\mathbf{M} = \begin{bmatrix} m_b & 0 & 0 \\ 0 & m_1 & 0 \\ 0 & 0 & m_2 \end{bmatrix} \quad (21)$$

$$\mathbf{C} = \begin{bmatrix} c_b + c_1 & -c_1 & 0 \\ -c_1 & c_1 + c_2 & -c_2 \\ 0 & -c_2 & c_2 \end{bmatrix} \quad (22)$$

$$\mathbf{K} = \begin{bmatrix} k_b(u_b(t), \dot{u}_b(t)) + k_1 & -k_1 & 0 \\ -k_1 & k_1 + k_2 & -k_2 \\ 0 & -k_2 & k_2 \end{bmatrix} \quad (23)$$

$$\mathbf{I} = \begin{Bmatrix} 1 \\ 1 \\ 1 \end{Bmatrix} \quad (24)$$

$$\ddot{\mathbf{u}}(t) = \begin{Bmatrix} \ddot{u}_b(t) \\ \ddot{u}_1(t) \\ \ddot{u}_2(t) \end{Bmatrix}, \dot{\mathbf{u}}(t) = \begin{Bmatrix} \dot{u}_b(t) \\ \dot{u}_1(t) \\ \dot{u}_2(t) \end{Bmatrix}, \mathbf{u}(t) = \begin{Bmatrix} u_b(t) \\ u_1(t) \\ u_2(t) \end{Bmatrix} \quad (25)$$

Numerically obtained acceleration-time history plots for the two-storey structure model, both fixed-base and base-isolated considered as 2-DOF and 3-DOF systems, respectively, are compared with the experimental data (see [28]) in Figures 7 and 8. Computed peak lateral accelerations recorded at the top of the analyzed two-storey structure model, with and without the PBs, are briefly reported in Table 4. Additionally, reduction levels in lateral accelerations are also presented and compared with the results of the previously performed shaking table investigation [28].

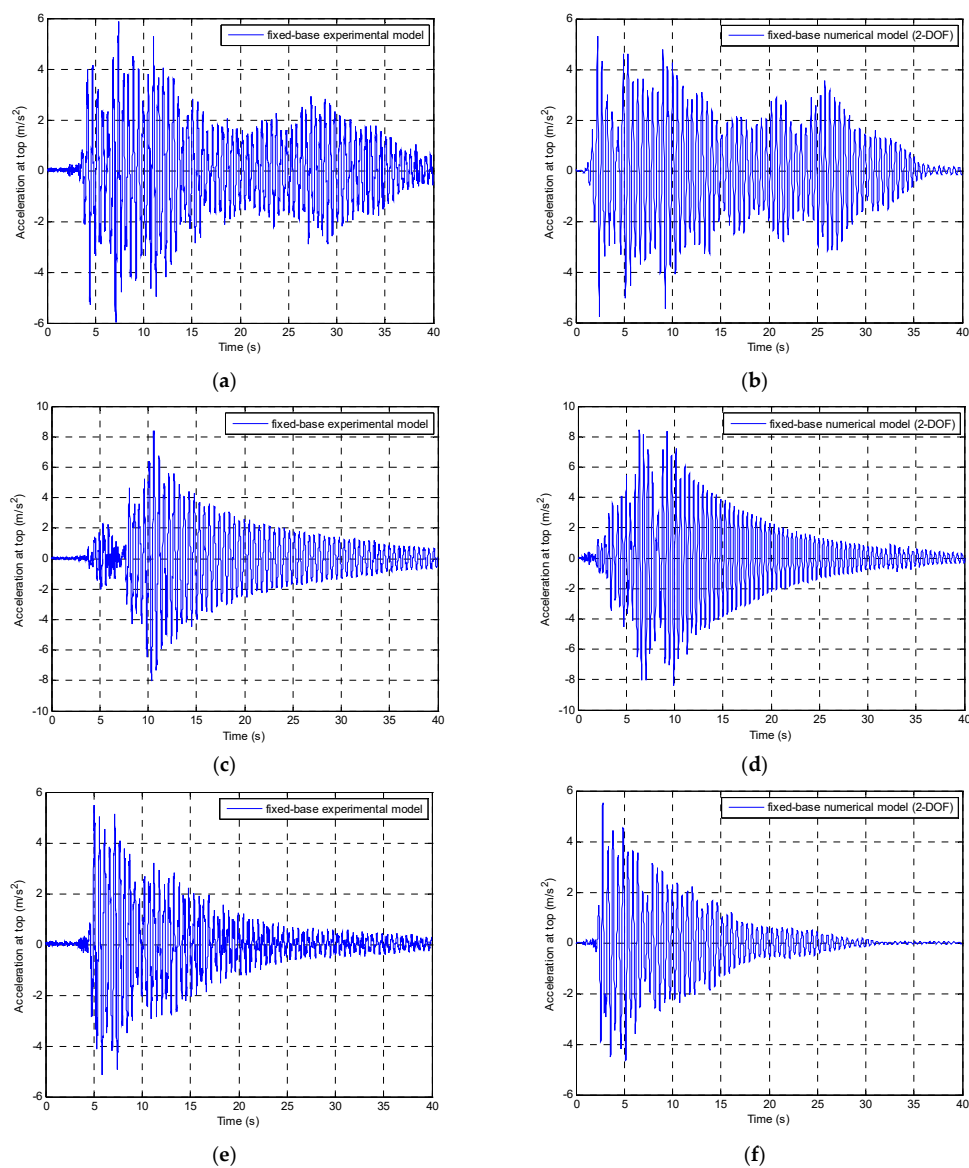


Figure 7. Cont.

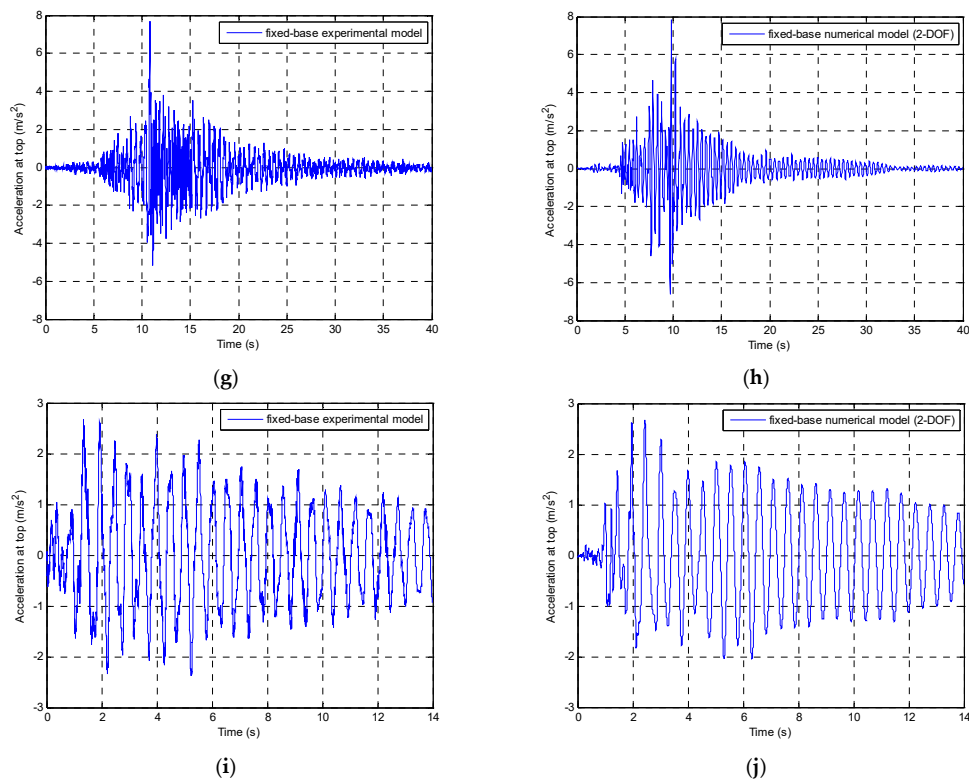


Figure 7. Experimentally determined (**left**) and numerically obtained (**right**) time-acceleration history plots for the fixed-base two-storey model during different ground motions: the 1940 El Centro earthquake (**a,b**), the 1971 San Fernando earthquake (**c,d**), the 1989 Loma Prieta earthquake (**e,f**), the 1994 Northridge earthquake (**g,h**), and the 2002 Polkowice mining tremor (**i,j**).

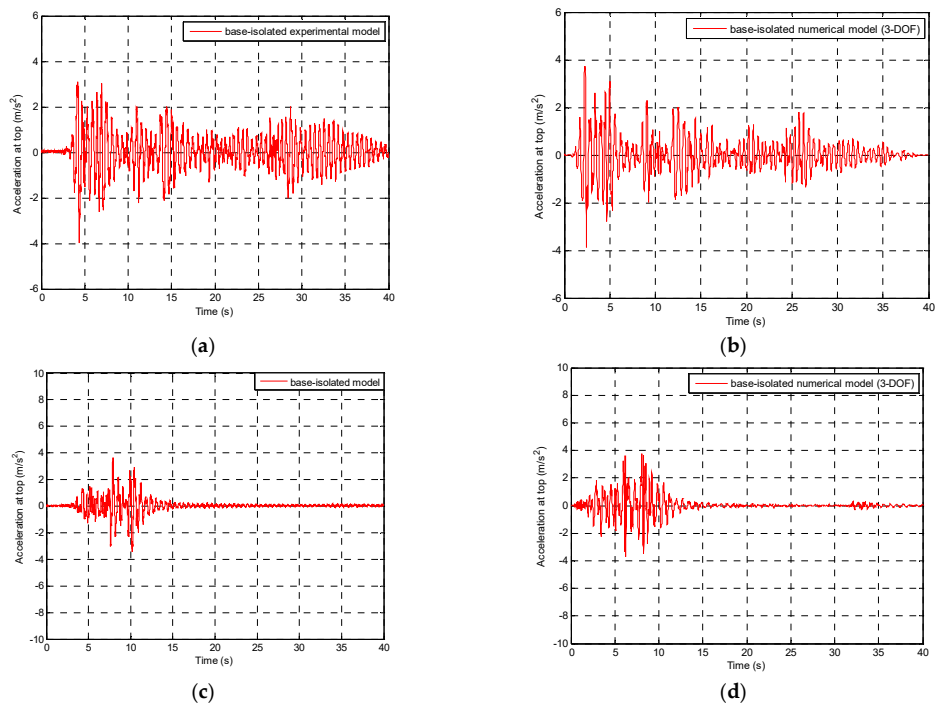


Figure 8. *Cont.*

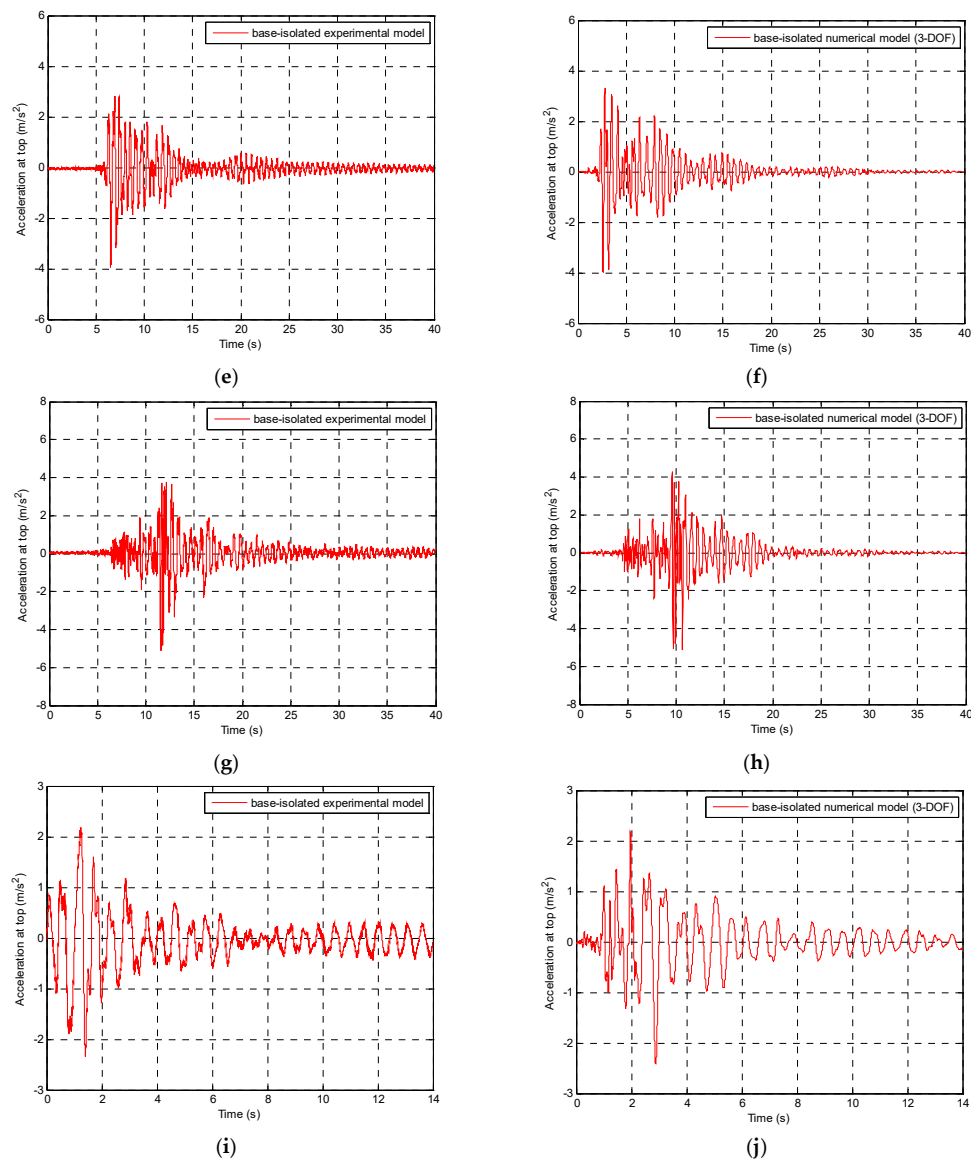


Figure 8. Experimentally determined (**left**) and numerically obtained (**right**) time-acceleration history plots for the base-isolated two-storey model during different ground motions: the 1940 El Centro earthquake (**a,b**), the 1971 San Fernando earthquake (**c,d**), the 1989 Loma Prieta earthquake (**e,f**), the 1994 Northridge earthquake (**g,h**), and the 2002 Polkowice mining tremor (**i,j**).

As indicated by Figures 5–8 and Tables 3 and 4, the results of the numerical analysis explicitly confirm high effectiveness of the developed mathematical model in simulating complex hysteretic behaviour of the prototype base isolation system made of PBs. Close inspection of Tables 3 and 4 demonstrates that the reduction levels in peak lateral accelerations, which were calculated based on both numerical results and previously obtained experimental data (see [28]), are very similar for every ground motion analyzed. In the case of the base-isolated single-storey model, the largest difference between numerical and experimental peak lateral acceleration has been obtained for the 1971 San Fernando earthquake (difference of 7.74%), while the lowest one for the 2002 Polkowice mining tremor (difference of 0.46%). On the other hand, in the case of the base-isolated two-storey model, the largest difference between numerical and experimental peak lateral acceleration has been obtained for the 1971 San Fernando earthquake (difference of 3.86%), while the lowest one for the 1994 Northridge earthquake (difference of 0.78%).

Table 4. Results of the seismic tests for the two-storey structure model.

Dynamic Excitation	Numerically Computed Peak Lateral Acceleration for the Two-Storey Structure Model (m/s ²)		Reduction Based on Numerical Analysis (%)	Reduction Based on Shaking Table Investigation (%) [28]
	Fixed-Base (2-DOF System)	Base-Isolated (3-DOF System)		
1940 El Centro earthquake NS component, original record with PGA = 3.070 m/s ²	5.77	3.89	32.58	33.3
1971 San Fernando earthquake Pacoima Dam station, N74°E component, scaled record with PGA = 5.688 m/s ²	8.45	3.77	55.38	56.8
1989 Loma Prieta earthquake Corralitos station, NS component, scaled record with PGA = 3.158 m/s ²	5.54	4.00	27.80	28.1
1994 Northridge earthquake Santa Monica station, EW component, scaled record with PGA = 4.332 m/s ²	7.85	5.10	35.03	33.1
2002 Polkowice mining tremor NS component, original record with PGA = 1.634 m/s ²	2.67	2.40	10.11	12.4

Where: PGA: Peak Ground Acceleration, NS: North-South, EW: East-West.

In addition to the peak lateral acceleration values, the whole time-acceleration records (Figures 5–8) were also compared and the difference between numerical and experimental results was assessed using the normalized mean square error. The error calculated for the base-isolated single-storey model for the 1940 El Centro, 1971 San Fernando, 1989 Loma Prieta, 1994 Northridge, and 2002 Polkowice ground motions is as low as 4.56%, 5.21%, 5.59%, 2.41% and 6.21%, respectively. On the other hand, the normalized mean square error calculated for the base-isolated two-storey model for the same suite of dynamic excitations is 7.26%, 5.88%, 7.89%, 6.71%, and 7.53%, respectively. The above results concerning the whole time-acceleration records indicate that the accuracy of the developed mathematical model somewhat drops for the two-storey structure model, which is believed to be triggered by more complex modelling related to the increased number of degrees of freedom. It should also be underlined that the set of function parameters a_1 – a_5 (incorporated in the numerical model) was evaluated to provide the best fit for the frequency range of 1 Hz to 5 Hz, which was taken as the most representative range for all ground motions considered in the present study. That approach has produced satisfactory results as the normalized mean square error has not exceeded 10% for all the earthquakes and the mining tremor analyzed in the research.

6. Conclusions

The paper reports the results of the comprehensive investigation designed to verify the effectiveness of an advanced mathematical model in simulating complex hysteretic behaviour of a prototype base isolation system made of PBs in numerical analysis. High effectiveness of PBs in reducing structural vibrations due to seismic excitations has already been experimentally confirmed during previously conducted shaking table investigation [28]. In the present paper, an advanced hysteretic model was developed to capture mechanical behaviour of PBs in numerical analysis. The effectiveness of the mathematical model was verified by comparing the previously obtained shaking table investigation data (i.e., seismic response of a single-storey and two-storey structure models under various ground motions) with the results of the detailed lumped-parameter analysis.

The results obtained from the investigation explicitly confirmed that the proposed mathematical model can be successfully adopted to accurately capture complex mechanical behaviour of PBs in numerical studies. They show that the reduction levels in peak lateral accelerations between numerical

and experimental results are very similar for all ground motions considered in the study. Moreover, relatively low normalized mean square errors were obtained when the whole time-acceleration numerical and experimental records were compared. It has to be also added that the results of the study indicated that the accuracy of the numerical analysis somewhat decreases as the number of DOFs increases.

The calibration procedure presented in the current investigation (performed by curve-fitting the general form of the developed mathematical model into the experimentally obtained hysteresis loops) was conducted for the prototype seismic isolation system made of PBs. Nevertheless, the preliminary experimental results obtained from the full-scale PBs, indicate that very similar shape of hysteresis loops can be observed. Therefore, the general form of the proposed mathematical model is expected to be also suitable for different PBs, regardless of their dimensions or scale factors. However, curve-fitting procedure has to be performed to evaluate a new set of function parameters for each specific PB.

Further development of the seismic isolation system made of full-scale PBs is to be performed. More studies are necessary to be conducted in order to fully verify the effectiveness of full-scale multi-dimensional PBs as a base isolation system for real structures. These should include detailed numerical simulations as well as experimental tests conducted on a large six degrees-of-freedom shaking table.

Author Contributions: Tomasz Falborski and Robert Jankowski conceived, designed and performed the numerical investigation presented in this paper. Tomasz Falborski analyzed the data and wrote the paper. Both authors discussed the results obtained and commented on the paper at all stages.

Conflicts of Interest: The authors declare no conflict of interest.

References

1. Jankowski, R.; Mahmoud, S. *Earthquake-Induced Structural Pounding*; Springer: Cham, Switzerland, 2015.
2. Naderpour, H.; Barros, R.C.; Khatami, S.M.; Jankowski, R. Numerical study on pounding between two adjacent buildings under earthquake excitation. *Shock Vib.* **2016**, 2016. [\[CrossRef\]](#)
3. Ebrahimian, M.; Todorovska, M.I.; Falborski, T. Wave Method for Structural Health Monitoring: Testing Using Full-Scale Shake Table Experiment Data. *J. Struct. Eng.* **2016**, 143. [\[CrossRef\]](#)
4. Kanyilmaz, A.; Castiglioni, C.A. Reducing the seismic vulnerability of existing elevated silos by means of base isolation devices. *Eng. Struct.* **2017**, 143, 477–497. [\[CrossRef\]](#)
5. Booth, E.; Key, D. *Earthquake Design Practice for Buildings*; Thomas Telford Publishing: London, UK, 2006.
6. Spencer, B.F.; Nagarajaiah, S. State of the Art of Structural Control. *J. Struct. Eng.* **2003**, 129, 845–856. [\[CrossRef\]](#)
7. Wolff, E.D.; Ipek, C.; Constantinou, M.C.; Tapan, M. Effect of viscous damping devices on the response of seismically isolated structures. *Earthq. Eng. Struct. D* **2015**, 44, 185–198. [\[CrossRef\]](#)
8. Pasala, D.T.R.; Sarlis, A.A.; Nagarajaiah, S.; Reinhorn, A.M.; Constantinou, M.C.; Taylor, D. Adaptive negative stiffness: New structural modification approach for seismic protection. *J. Struct. Eng.* **2012**, 138, 1112–1123. [\[CrossRef\]](#)
9. Symans, M.D.; Constantinou, M.C. Semi-active control systems for seismic protection of structures: A state-of-the-art review. *Eng. Struct.* **1999**, 21, 469–487. [\[CrossRef\]](#)
10. Naeim, F.; Kelly, J.M. *Design of Seismic Isolated Structures: From Theory to Practice*; John Wiley and Sons: New York, NY, USA, 1999.
11. Housner, G.W.; Bergman, L.A.; Caughey, T.K.; Chassiakos, A.G.; Claus, R.O.; Masri, S.F.; Skelton, R.E.; Soong, T.T.; Spencer, B.F.; Yao, J.T.P. Structural control: Past, present, and future. *J. Eng. Mech.* **1997**, 123, 897–971. [\[CrossRef\]](#)
12. Komodromos, P. *Seismic Isolation of Earthquake-Resistant Structures*; WIT Press: Southampton, UK, 2000.
13. Kelly, J.M. Base isolation: Linear theory and design. *Earthq. Spectra* **1990**, 6, 223–244. [\[CrossRef\]](#)
14. Buckle, I.G.; Mayes, R.L. Seismic isolation: History, application, and performance: A world view. *Earthq. Spectra* **1990**, 6, 161–201. [\[CrossRef\]](#)
15. Mavronicola, E.; Komodromos, P. On the response of base-isolated buildings using bilinear models for LRBs subjected to pulse-like ground motions: Sharp vs. smooth behaviour. *Earthq. Struct.* **2014**, 7, 1223–1240. [\[CrossRef\]](#)

16. Kumar, M.; Whittaker, A.S.; Constantinou, M.C. Characterizing friction in sliding isolation bearings. *Earthq. Eng. Struct. Dyn.* **2015**, *44*, 1409–1425. [[CrossRef](#)]
17. Fenz, D.M.; Constantinou, M.C. Behaviour of the double concave friction pendulum bearing. *Earthq. Eng. Struct. Dyn.* **2006**, *35*, 1403–1424. [[CrossRef](#)]
18. Mokha, A.; Constantinou, M.C.; Reinhorn, A.M.; Zayas, V.A. Experimental study of friction-pendulum isolation system. *J. Struct. Eng.* **1991**, *117*, 1201–1217. [[CrossRef](#)]
19. Nagarajaiah, S.; Xiaohong, S. Seismic performance of base-isolated buildings in the 1994 Northridge earthquake. In Proceedings of the 11th World Conference on Earthquake Engineering, Acapulco, Mexico, 23–28 June 1996.
20. Nagarajaiah, S.; Xiaohong, S. Response of base-isolated USC hospital building in Northridge earthquake. *J. Struct. Eng.* **2000**, *126*, 1177–1188. [[CrossRef](#)]
21. Kumar, M.; Whittaker, A.S.; Constantinou, M.C. An advanced numerical model of elastomeric seismic isolation bearings. *Earthq. Eng. Struct. Dyn.* **2014**, *43*, 1955–1974. [[CrossRef](#)]
22. Yamamoto, S.; Kikuchi, M.; Ueda, M.; Aiken, I.D. A mechanical model for elastomeric seismic isolation bearings including the influence of axial load. *Earthq. Eng. Struct. Dyn.* **2009**, *38*, 157–180. [[CrossRef](#)]
23. Hwang, J.S.; Wu, J.D.; Pan, T.C.; Yang, G. A mathematical hysteretic model for elastomeric isolation bearings. *Earthq. Eng. Struct. Dyn.* **2002**, *31*, 771–789. [[CrossRef](#)]
24. Kikuchi, M.; Aiken, I.D. An analytical hysteresis model for elastomeric seismic isolation bearings. *Earthq. Eng. Struct. Dyn.* **1997**, *26*, 215–231. [[CrossRef](#)]
25. Tsai, C.S.; Chiang, T.C.; Chen, B.J.; Lin, S.B. An advanced analytical model for high damping rubber bearings. *Earthq. Eng. Struct. Dyn.* **2003**, *32*, 1373–1387. [[CrossRef](#)]
26. Jankowski, R. Nonlinear rate dependent model of high damping rubber bearing. *Bull. Earthq. Eng.* **2003**, *1*, 397–403. [[CrossRef](#)]
27. Falborski, T.; Jankowski, R.; Kwiecień, A. Experimental study on polymer mass used to repair damaged structures. *Key Eng. Mater.* **2012**, *488*, 347–350. [[CrossRef](#)]
28. Falborski, T.; Jankowski, R. Experimental study on effectiveness of a prototype seismic isolation system made of Polymeric Bearings. *Appl. Sci.* **2017**, *7*, 808. [[CrossRef](#)]
29. Chopra, A.K. *Dynamics of Structures: Theory and Applications to Earthquake Engineering*; Prentice Hall: Englewood Cliffs, NJ, USA, 2012.
30. Maciag, E.; Kuzniar, K.; Tatara, T. Response spectra of ground motions and building foundation vibrations excited by rockbursts in the LGC region. *Earthq. Spectra* **2016**, *32*, 1769–1791. [[CrossRef](#)]
31. Zembaty, Z. Rockburst induced ground motion—a comparative study. *SDEE* **2004**, *24*, 11–23. [[CrossRef](#)]



© 2018 by the authors. Licensee MDPI, Basel, Switzerland. This article is an open access article distributed under the terms and conditions of the Creative Commons Attribution (CC BY) license (<http://creativecommons.org/licenses/by/4.0/>).